Journal of
Synchrotron Radiation

ISSN 0909-0495

Received 17 October 2005
Accepted 18 January 2006

Silicon drift and pixel devices for X-ray imaging and spectroscopy

G. Lutz

MPI-Halbleiterlabor, Otto Hahn Ring 6, D-81739 München, Germany.
E-mail: gerhard.lutz@hll.mpg.de

Starting from the basic photon detection process in semiconductors, the function, principles and properties of sophisticated silicon detectors are discussed. These detectors are based on, or inspired by, the semiconductor drift detector. They have already shown their potential in X-ray astronomy (pn-CCD) and in X-ray spectroscopy (silicon drift diode), and further detector types (DEPFET pixel detector and macro-pixel detector) are under development for several other future experiments. The detectors seem to be very well suited for synchrotron radiation experiments.

© 2006 International Union of Crystallography
Printed in Great Britain – all rights reserved

Keywords: semiconductor detector; silicon drift detector; pixel detector; CCD; DEPFET; X-ray detection; X-ray spectroscopy; X-ray imaging.

1. Introduction

Semiconductor detectors, and in particular silicon detectors, are very well suited for detection and measurement of ionizing radiation caused by interaction with charged particles and (X-ray) photons. Precise position, time and energy measurement can be combined when use is made of the excellent intrinsic material properties in well thought-out detector concepts. This is done in silicon drift detectors and several other inventions which have already found their way into scientific and other applications. Although development and large-scale use of modern silicon detectors has been initiated in particle physics, this presentation will concentrate on (X-ray) single-photon detection.

2. Basic detection process of single photons in semiconductors

The simplest detector is a reversely biased diode (Fig. 1). Photons interacting in silicon will, depending on their energy, produce one or more electron–hole pairs. An average energy of 3.6 eV is needed for creation of a pair in silicon with a band gap of 1.12 eV. This should be compared with the ionization energy of gases which is an order of magnitude higher. Electrons and holes will be separated by the electric field within the space charge region and collected at the electrodes on opposite sides of the diode.

The small band gap and the corresponding large signal charge generated in the photon absorption process is the principal cause of the excellent properties of semiconductor radiation detectors manifesting themselves in particular in very good spectroscopic resolution down to low energies. Further reasons are the high density and corresponding low range of δ-electrons which makes very precise position measurement possible. High charge carrier mobility combined with small detector volume leads to short charge collection time and makes the use of detectors in a high rate environment possible. The excellent mechanical rigidity makes the use of gas containment foils superfluous and allows operation in a vacuum. Therefore very thin entrance windows can be constructed and high quantum efficiency can be reached down to low energies. Space-dependent doping of semiconductors allows construction of detectors with sophisticated electric field configurations and intrinsically new properties.

Reaching all these good detector properties requires readout electronics which are well matched to the detectors. Here we notice a point specific to silicon which is also the basic material of most of present day electronics. For this reason it is natural to integrate the sensitive front-end part of the electronics into the detector. This is the case, for example, in CCDs and drift diodes with very high spectroscopic resolution. A further device (DEPFET) combines the function of detector and amplifier in the basic structure.

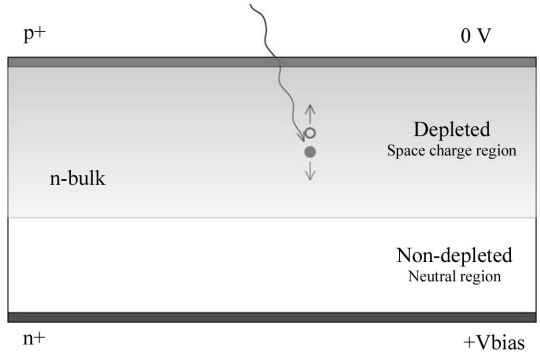

Figure 1
Schematic structure of a reversely biased semiconductor diode used as a photon detector and connected to a readout amplifier.

3. Detector principles

The detectors described in this section are based on, or at least inspired by, the semiconductor drift chamber which was invented by Emilio Gatti and Pavel Rehak (Gatti & Rehak, 1984). This device (Fig. 2) makes use of the sideward depletion principle, having diode junctions on both surfaces and a bulk contact on the fringe. Fully depleting the device by applying a reverse bias voltage between p- and n-contacts creates an electron potential valley in the middle plane. Electrons created by an interacting photon will assemble in this valley and subsequently diffuse until they eventually reach the n-doped anode. Faster and controlled collection is reached by adding a horizontal drift field. This is done by dividing the diodes into strips and applying raising voltages from strip to strip. This device is able to measure position (by means of the time difference between particle interaction and arrival of the signal at the anode) as well as energy. In most applications the latter aspect is the important one. Here one profits from the small electric capacitance of the anode which acts as a capacitive load to the readout amplifier. Large area detectors can therefore be operated with high energy resolution at high data rate.

By operating the same basic structure in a different way one arrives at the pn-CCD (Kemmer & Lutz, 1987*a*, 1988; Strüder *et al.*, 1987) (Fig. 3). Instead of having a continually rising potential from strip to strip, a periodically modulated potential is applied with a periodicity of three strips and the electron potential valley is moved close to the top side by applying a more negative potential to the back p^+ contact. This way the valley is modulated in depth and there is no need to structure the diode on the back of the wafer. The large-area diode may serve as entrance window for the radiation. As was the case for the drift detector, the substrate is fully depleted and the detector is sensitive over the full wafer thickness. Having a large sensitive thickness is important for detection of photons in the elevated energy range.

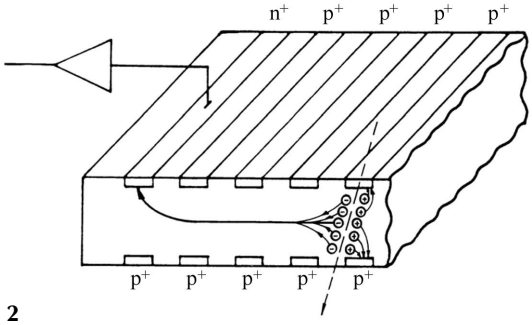

Figure 2
Semiconductor drift chamber structure using the sideward depletion method. Dividing the diode into strips and applying a continuously rising potential superimposes a horizontal field that drives the signal electron towards the n^+ anode which is connected to the readout electronics. Upon arrival of the signal charge at the n^+ anode, the amount of charge and the arrival time can be measured.

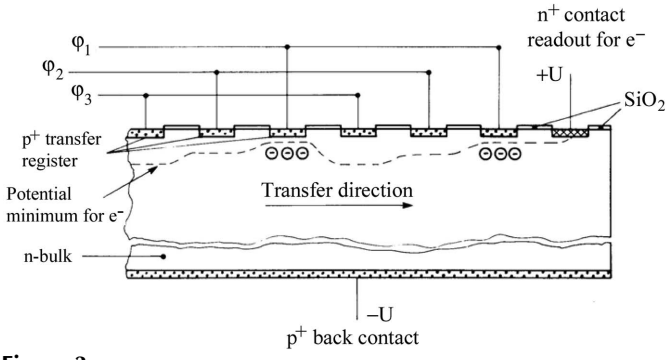

Figure 3
The fully depleted pn-CCD: cross section along the channel.

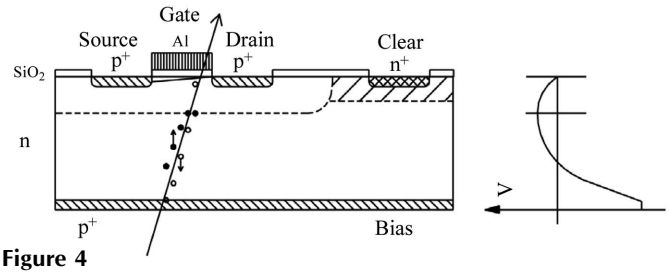

Figure 4
The concept of a DEPFET: simplified device structure (left) and potential distribution along a cut across the wafer in the gate region of the transistor (right).

The DEPFET structure, which simultaneously possesses detector and amplification properties, was proposed by J. Kemmer and G. Lutz in 1987 (Kemmer & Lutz, 1987*a*, 1988) and has subsequently been confirmed experimentally (Kemmer *et al.*, 1990). It is based on the combination of the sideward depletion method, as used in a semiconductor drift chamber shown in Fig. 2, and the field effect transistor principle.

In Fig. 4, a p-channel transistor is located on a fully depleted n-type bulk. As with the pn-CCD, the potential valley has been moved close to the top side. Signal electrons generated in the fully depleted bulk assemble in a potential maximum ('internal gate') and increase the transistor channel conductivity by induction. The device can be reset by applying a large positive voltage on the clear electrode.

The DEPFET has several interesting properties: (i) combined function of sensor and amplifier; (ii) full sensitivity over complete wafer; (iii) low capacitance and low noise; (iv) non-destructive repeated readout; (v) complete clearing of signal charge: no reset noise. These properties make it an ideal building block for an X-ray pixel detector.

4. Silicon drift detectors: structures and properties

A variety of drift detectors have been developed and adapted to specific applications. Of great importance is the drift diode (Kemmer & Lutz, 1987*a*,*b*; Kemmer *et al.*, 1987), a device with an unstructured homogeneous radiation entrance window (Fig. 5). Further significant improvement was obtained by integrating a readout transistor into the device (Fig. 6). In contrast to the original drift chamber with the electron potential valley located parallel to the wafer surfaces, now only one structured surface provides the drift field in the valley which is now at an angle with respect to the wafer surface.

Having only one surface structured brings about the possibility of using the unstructured surface of the fully depleted device as radiation entrance window. Not having to take other functions into consideration, this radiation entrance window can be made very thin and homogeneous (Hartmann *et al.*, 1997). Using circular geometry with a very small charge-collecting anode in its centre reduces the capacitive load to the amplifier and therefore the noise.

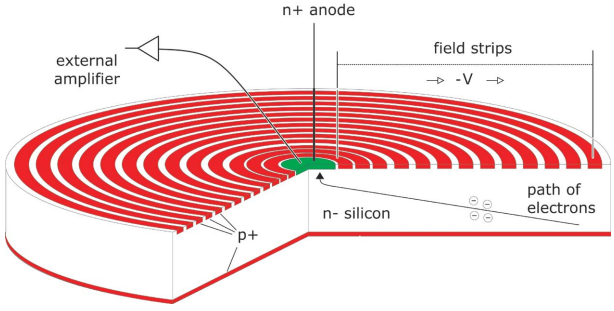

Figure 5
Cylindrical silicon drift chamber with an integrated amplifier for spectroscopic applications. The entire silicon wafer is sensitive to radiation. Electrons are guided by an electric field towards the small-sized collecting anode in the centre of the device.

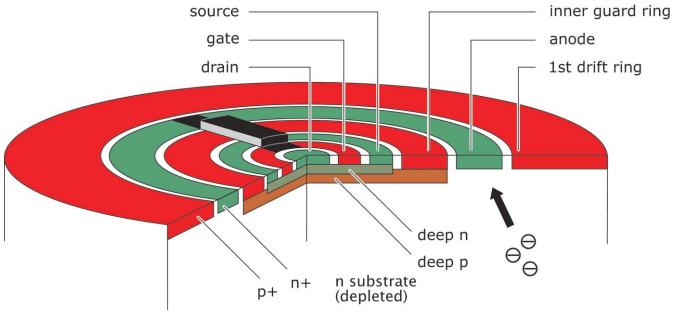

Figure 6
On-chip single-sided junction FET coupled to the readout node of a silicon drift detector.

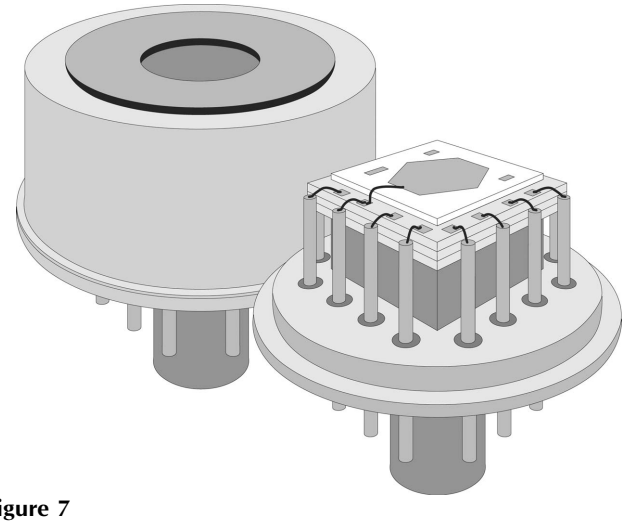

Figure 7
Perspective view of a module consisting of a single-sided structured cylindrical drift detector with integrated SSJFET transistor, cooled by a Peltier element.

Having the first transistor integrated into the device (Hartmann *et al.*, 1994), the capacitance of the detector–amplifier system is minimized by eliminating bond wires between detector and amplifier, thus avoiding all kinds of stray capacitances between the readout node and ground, making the system again faster and less noisy. Further advantages are evident as the effect of electrical pick-up is significantly reduced and problems of microphony, *i.e.* noise introduced by mechanical vibration, are excluded. In order to be able to work on the lowly doped and fully depleted substrate, a non-standard single-sided junction field effect transistor (SSJFET) had to be developed (Radeka *et al.*, 1989; Pinotti *et al.*, 1993).

Silicon drift diodes (SDDs) with integrated transistor are now commercially available. They can also be obtained as modules assembled with a Peltier cooler in a gas-tight housing with thin radiation entrance window (Fig. 7). To demonstrate the excellent spectroscopic properties achieved with such devices, Fig. 8 presents a spectrum obtained with a ^{55}Fe source and the quantum efficiency for a cylindrical SDD with a sensitive area of 5 mm^2. The detector temperature, important for the leakage current, was set to 253 K and the signal shaping time to 1 µs. The $Mn_{K\alpha}$ peak at 5.9 keV and $Mn_{K\beta}$

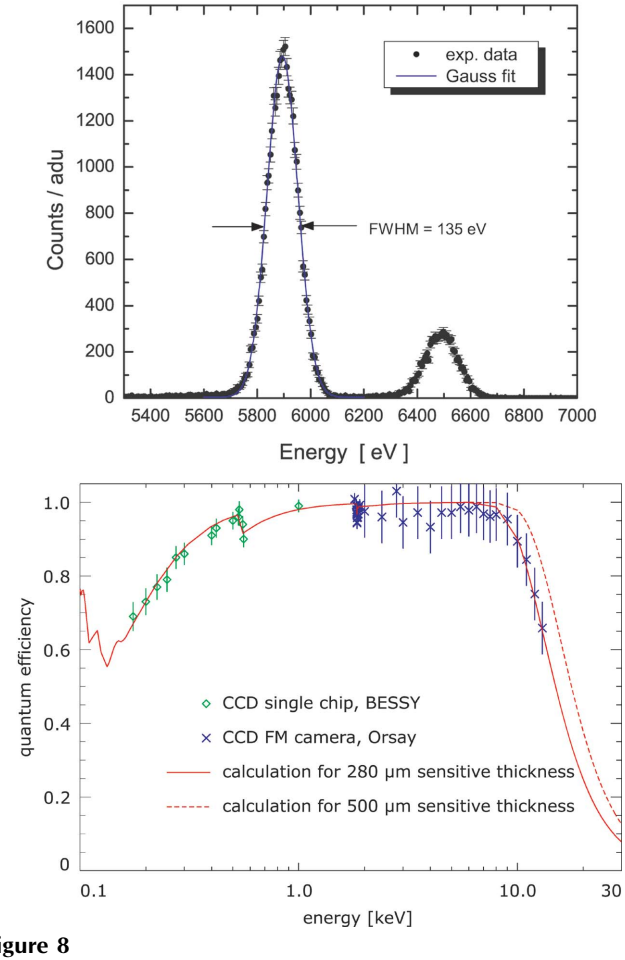

Figure 8
$Mn_{K\alpha}$ – $Mn_{K\beta}$ spectrum (top) and quantum efficiency (bottom) of a 5 mm^2 drift diode. The device was operated at 253 K and at a shaping time of 1 µs.

Table 1
Properties of commercially available drift detectors (PnSensor GmbH).

Geometry	Active volume	Energy resolution FWHM @ 5.9 keV at T = 263 K	Energy resolution FWHM @ 5.9 keV at T = 253 K	Peak/background ratio
Symmetric	5 mm^2 × 450 µm	143–153 eV	138–143 eV	1500
Symmetric	10 mm^2 × 450 µm	148–158 eV	140–145 eV	3000
Symmetric	20 mm^2 × 450 µm	145 eV	135 eV	3000–5000
Symmetric	30 mm^2 × 450 µm	150 eV	140 eV	3000–5000
Symmetric	5 mm^2 × 450 µm	145 eV	133 eV	7000–10000
Symmetric	10 mm^2 × 450 µm	135 eV	128 eV	7000–10000

Table 2
Properties of some commercially available silicon drift detectors compared with lithium drifted silicon diodes [Si(Li)] and high-purity germanium (HPGe) detectors.

Detector type	Cooling method	Thickness (mm)	Active area (mm^2)	FWHM Mn $K\alpha$ *versus* count rate (eV)			Maximum rate (kcps)
				1 kcps	50 kcps	1 Mcps	
Si(Li)	Liquid nitrogen	3 to 5	10 to 200	129	190	–	30 to 50
HPGe	Liquid nitrogen	3	10 to 20	109	175	–	30 to 50
Si drift	Peltier 253 K	0.3 to 0.5	5 to 100	145	160	260	400

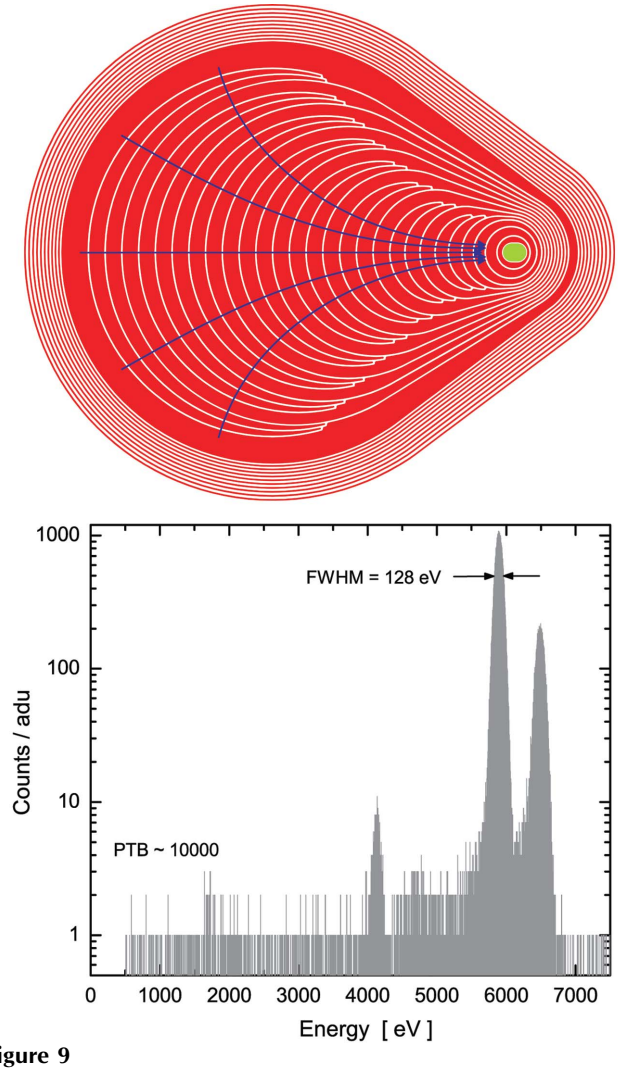

Figure 9
Asymmetric drift diode (droplet geometry) with anode and transistor moved outside of the sensitive area: geometry (top) and ^{55}Fe spectrum (bottom). A very high peak-to-background ratio is reached.

peak at 6.5 keV are clearly separated and their widths are only slightly above the intrinsic Fano limit given by the pair generation process in silicon.

Cylindrical drift diodes with integrated SSJFETs have been manufactured with sensitive areas in the range from 5 mm^2 to 1 cm^2. Important for a good signal-to-background ratio is complete charge collection for each individual photon. Incomplete charge collection for a fraction of photons leads to a low energy tail in the spectrum. This is the case for photons converting close to the entrance window and also for those entering the rim region or a very small region in the centre below the integrated transistor. In the first case, electron–hole recombination in the surface region is responsible while in the small centre region some electrons may reach the clear contact instead of the collecting anode. The rim region can be shielded by a collimator. A 'droplet' geometry (Fig. 9) avoids the second problem (Lechner *et al.*, 2003). Here the collecting anode and the transistor are placed outside the sensitive region defined by a collimator. Correspondingly, a very high peak-to-valley ratio (10000) is reached. Table 1 compiles results of properties obtained with silicon drift detectors of various types, and Table 2 compares silicon drift detectors with other types of semiconductor detectors.

The devices described so far have been optimized for spectroscopic performance only. Position sensitivity may be obtained by arranging drift diodes in a matrix-like fashion (Gauthier *et al.*, 1996; Fiorini *et al.*, 2002) as shown in Fig. 10. These arrangements are especially useful when attached to a

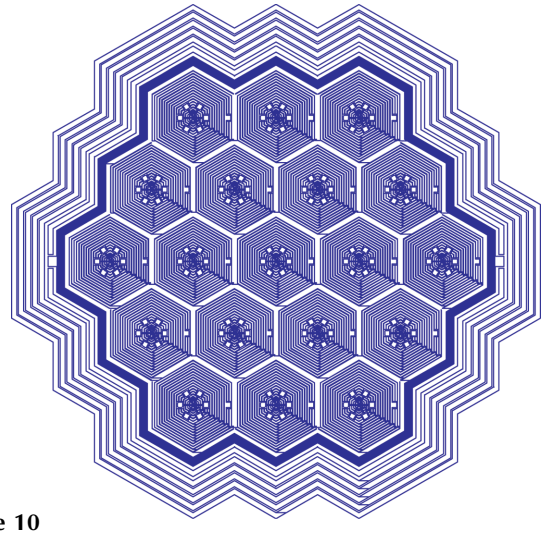

Figure 10
Multichannel drift detector consisting of 19 hexagonal 5 mm^2 SDDs.

scintillating crystal (Fiorini *et al.*, 1999). Scintillation light will be spread over more than one cell and the position of the photon can be determined by the ratio of the signals. Using scintillating crystals as photon absorber extends the energy range far above that possible with interactions in silicon. Fig. 11 shows such an arrangement together with the reconstructed photon positions obtained from a 122 keV X-ray exposure through a mask with six pinholes. A 3 mm-thick CsI(Tl) crystal leads to an efficiency of 80%. The gain was 15.4 electrons keV^{-1} and the energy resolution was 17.4% full width at half-maximum (FWHM) at 122 keV. The position resolution was determined as 0.25 mm FWHM.

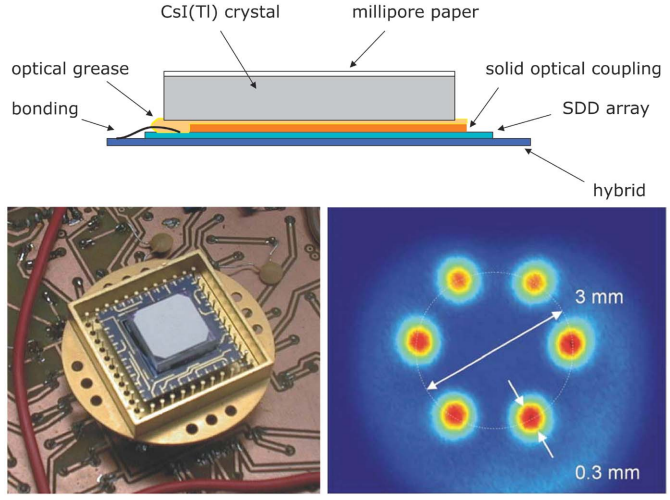

Figure 11
Multichannel drift detector optically coupled to a CsI(Tl) scintillating crystal: arrangement (top), photograph (left) and distribution of reconstructed photons from illumination through a pin-hole mask (right).

5. The pn-CCD: X-ray imaging and spectroscopy

Pn-CCDs were originally developed for X-ray imaging in space. A 6 cm × 6 cm device is used as focal imager in one of the three X-ray mirror telescopes at the European XMM/Newton X-ray observatory (Meidinger *et al.*, 1999). Since the beginning of 2000 it has been producing high-quality X-ray images of the sky (Strüder *et al.*, 2003).

The principle, derived from the silicon drift chamber, has already been shown in Fig. 3. The layout of the XMM focal plane detector is shown in Fig. 12. Twelve 1 cm × 3 cm CCDs with 150 µm × 150 µm pixel size are monolithically integrated into a single device placed on a 4-inch silicon wafer of thickness 300 µm. Each column of pixels has its own readout channel so as to allow fast parallel readout of the device.

Fig. 13 shows a cross section through the CCD along the transfer channel. Here one sees in greater detail the functioning of the device. Contrary to standard MOS-CCDs the registers are formed as pn-junctions and the radiation-sensitive oxide plays only a peripheral role. The device is fully depleted with increased n-type doping concentration in the epitaxic layer beneath the top surface. This leads to a potential distribution shown in the right-hand part of the figure and prevents holes from the p+ doped registers to be emitted across the wafer towards the back p-doped entrance window. Charge storage and transfer occurs in a depth of approximately 10 µm in contrast to MOS CCDs where this happens at the silicon–oxide boundary. Fast charge transfer (by drift) is therefore possible up to large pixel sizes.

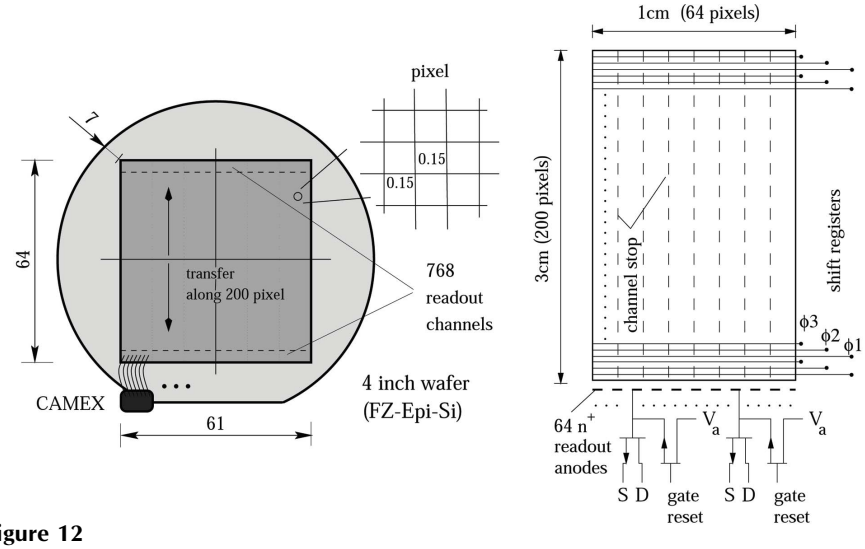

Figure 12
Layout of the XMM pn-CCD. Twelve logically separate pn-CCDs of area 1 cm × 3 cm are monolithically combined on a 4-inch wafer to a 6 cm × 6 cm device with common back entrance window. The pixel size is 150 µm × 150 µm.

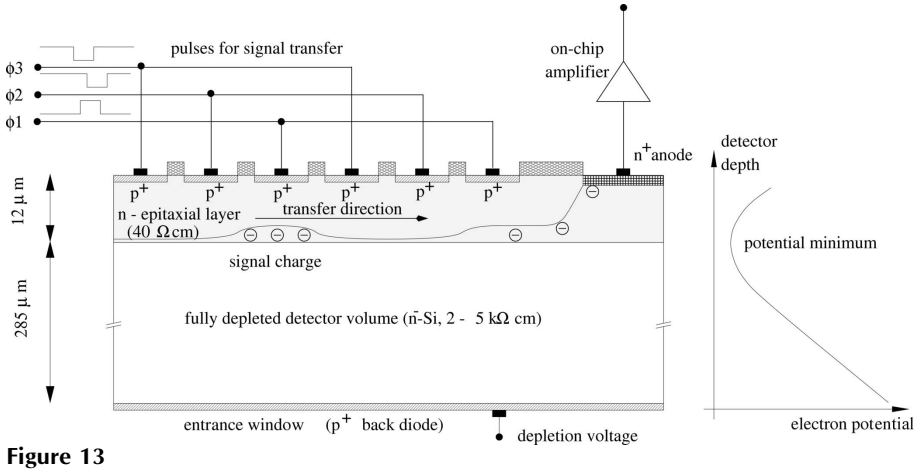

Figure 13
A schematic cross section through the pn-CCD along a transfer channel. The device is back illuminated and fully depleted over 300 µm thickness. The electron potential perpendicular to the wafer surface is shown on the right-hand side.

The excellent combined imaging and spectroscopic capabilities of the pn-CCD are demonstrated in Fig. 14, which shows an X-ray image of the remnant of the supernova observed by Tycho Brahe in 1572. Overlaid is the spectrum with prominent lines of various elements in high ionization stages. Table 2 summarizes the properties of the XMM pn-CCD.

For further proposed missions [*i.e.* DUO (Dark Universe Observatory) and ROSITA (Roentgen Survey with an Imaging Telescope Array)], significantly improved pn-CCDs have been developed (Meidinger *et al.*, 2006). In addition to the radiation-sensitive image areas, they possess frame store areas (Fig. 15). Images collected during integration time can be rapidly shifted from the image to the frame store area and then read out with reduced speed while simultaneously collecting the next image. The pixel size has been reduced to 51 µm × 51 µm and 75 µm × 75 µm, and various other improvements have been implemented. A noise figure of 1.8 electrons (r.m.s.) enables measurements down to very low energies. Figs. 16 and 17 show the spectra of ^{55}Fe and the carbon *Kα* line at 277 eV well separated from the tail of electronic noise.

Important properties of XMM- and ROSITA-type pn-CCDs are summarized in Table 3. Also included in this table are the properties obtained with prototype DEPFET pixel detectors to be described in the following section and intended for use in the European XEUS X-ray observatory.

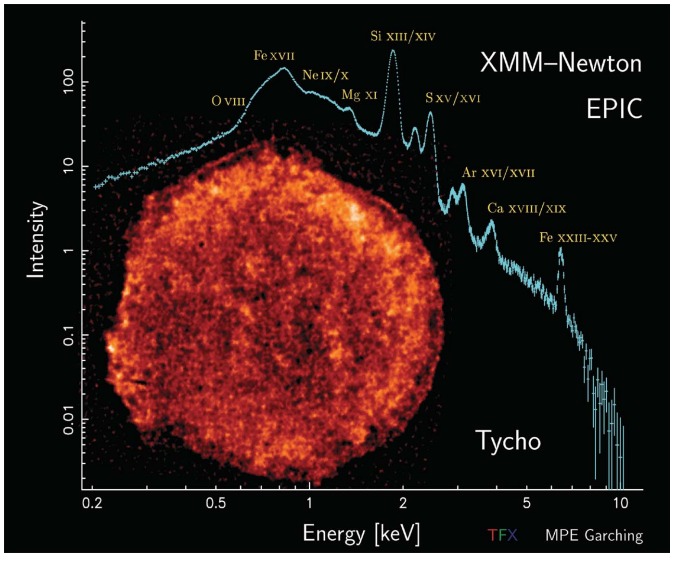

Figure 14
Supernova remnant Tycho in the Cassiopeia region, discovered in 1572 by Tycho Brahe. The radius of Tycho is 12 light years. The temperature of about one million degrees gives rise to X-rays from 0.2 keV to 10 keV. The X-ray spectrum shows an abundance of many elements, among them O, Mg, Si, S, Ar, Ca, Fe and Ni.

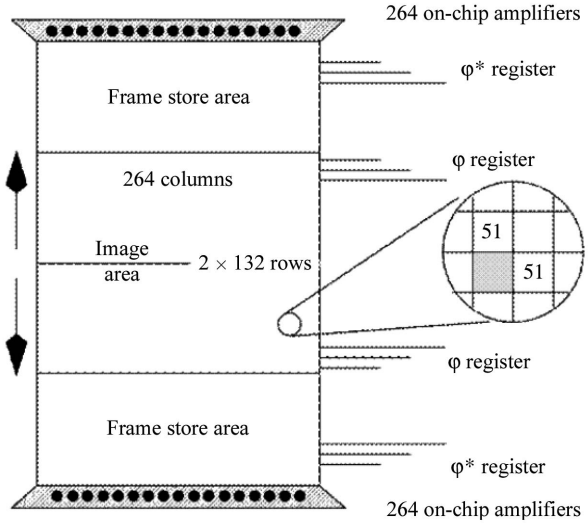

Figure 15
Example of a pn-CCD operated in a frame store mode. The imaging area has pixel sizes of 51 µm × 51 µm or 75 µm × 75 µm and the store area of 75 µm × 50 µm.

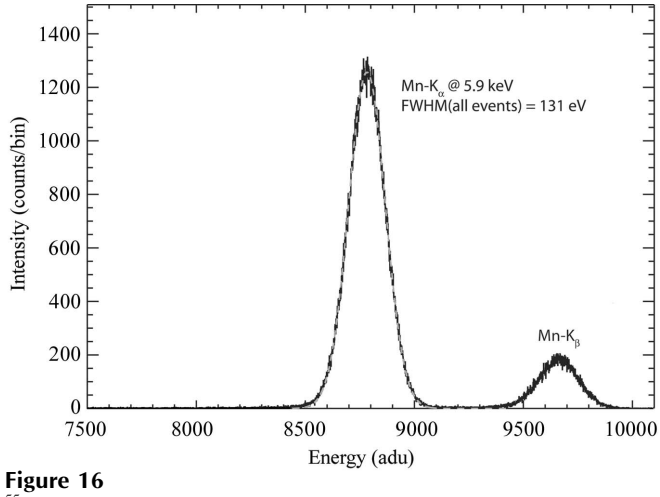

Figure 16
^{55}Fe spectrum measured with the frame store pn-CCD at 190 K. Owing to the small (in comparison to XMM) 75 µm × 75 µm pixel size the signal charge is usually spread to more than one pixel. A FWHM of 120 eV is obtained when one selects events in which all charge is contained in a single pixel. By allowing a spread into up to four pixels, one obtains a FWHM of 131 eV.

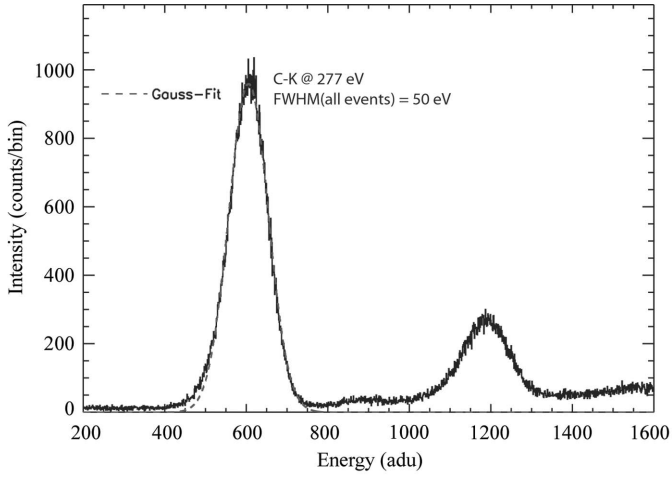

Figure 17
Carbon and oxygen spectrum measured with the frame store pn-CCD at 233 K. A FWHM of 50 eV is obtained for the carbon *Kα* line at 277 eV.

Table 3
Comparison of expected properties of pn-CCDs in ROSITA with those reached at XMM.

The energy resolution (FWHM) refers to incident X-rays of the Mn *K* line at 5.9 keV and measured at temperatures of ∼173 K.

	XMM	ROSITA	XEUS
Status	Operating in orbit	Produced and tested	Prototypes tested
Type	Full frame	Frame store	DEPFET pixel sensors
Format	400 × 384	256 × 256	1024 × 1024
Pixel size	150 µm × 150 µm	75 µm × 75 µm	50 µm × 50 µm or 75 µm × 75 µm
Readout noise	5 electrons	3 electrons	3 electrons
Sensitive thickness	295 µm	450 µm	450 µm
Frame rate	15 frames s^{-1}	20 frames s^{-1}	500 frames s^{-1}
Readout speed	350 ns $pixel^{-1}$	100 ns $pixel^{-1}$	50 ns $pixel^{-1}$
Energy resolution at Mn *Kα* (5.9 keV)	150 eV	130 eV	125 eV
Operating temperature	173 K	213 K	233 K
Energy resolution at C *Kα*	130 eV	80 eV	45 eV
Energy range	0.15–15 keV	0.1–20 keV	0.05–20 keV

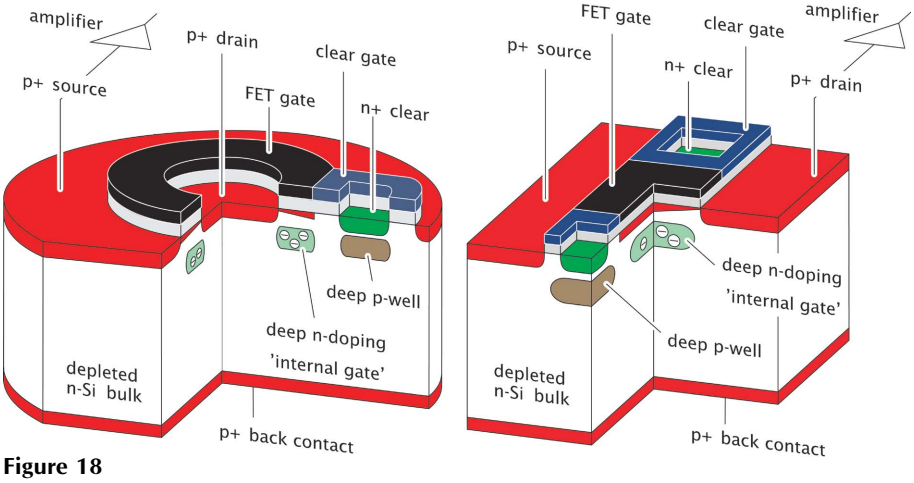

Figure 18
Schematic drawings of MOS-type DEPFETs with circular (left) and linear (right) geometry. Signal charge is collected in a potential well (internal gate) below the FET gate, thereby increasing the conductivity of and current within the transistor channel. Collected charges can be drained towards the clear contact by applying voltage pulses to the clear contact and/or the clear gate.

6. DEPFET active pixel sensors

The depleted field effect transistor structure shown in Fig. 4 is a natural building element for a pixel detector. It acts simultaneously as detector and as amplifier. A variety of DEPFETs can be constructed. Fig. 18 shows two examples, one with cylindrical and the other with linear geometry.

By arranging many of these devices in a matrix-like fashion and connecting them in such a way that selected DEPFETs can be turned, one arrives at a pixel detector with charge-storing capability. Before turning to the matrix arrangement the important properties of the DEPFETs are:

(i) Combined function of sensor and amplifier.

(ii) Full sensitivity over complete wafer.

(iii) Low capacitance and low noise.

(iv) Non-destructive repeated readout.

(v) Complete clearing of signal charge: no reset noise. Possibility of repeated readout of the same signal as reading does not involve destruction of signal charge.

(vi) A variety of types and topologies can be employed: MOSFET, JFET; enhancement and depletion types; linear and cylindrical geometries; several types of clear structures.

(vii) Continuous (real time) and integrating (charge storage) operation modes can be chosen.

The signal can be read out either at the source as indicated in the left-hand figure or at the drain as shown in the linear example. With source follower readout one compensates the increase of channel conduction due to the charge in the internal gate by a reduction of the external gate-source voltage, seen as voltage change of the source. In the drain readout configuration the source potential is kept constant and the drain current change can be directly observed. A very important property in pixel detector applications is the fact that signal charge collection occurs not only for current-carrying DEPFETs but also for those which have been turned off with the help of the external FET gate.

DEPFET pixel sensors are being developed at the MPI Semiconductor Laboratory in Munich for two purposes, as focal sensors of the proposed European X-ray observatory XEUS (XEUS, 1999) and as vertex detector for the proposed International Linear Collider (ILC). In XEUS the combined functions of imaging and spectroscopy are of importance; for ILC only the measurement of position of charged tracks passing through the detectors are of interest. This, however, has to be done with very high precision (few µm) and at very high readout speed. The position measurement requirement in XEUS is not as stringent, it is matched to the expected quality of X-ray imaging. However, highest emphasis is given to spectroscopic quality and quantum efficiency, and data readout speed is still unusually large.

As a consequence of these and further requirements, circular geometries have been chosen for XEUS and linear ones for ILC (see Fig. 18). The excellent spectroscopic capabilities of DEPFETs can be appreciated from the ^{55}Fe source spectrum taken with a single circular pixel cell (Fig. 19).

The DEPFET, with its capability of creating, storing and amplifying signal charge, is an ideal building block for a pixel detector. A large number of DEPFETs can be arranged in a matrix-like form in such a way as to power selected DEPFETs for reading and clearing the collected signal charge. Fig. 20 shows a rectangular arrangement of DEPFETs. Their drains are connected in a column-wise fashion while gates and clear electrodes are connected row-wise. Each row has its individual readout electronics channel. A row at a time is turned on with the help of the gate voltage while all other DEPFETs have zero current. Charge collection does not require current within the DEPFET.

Readout can be performed in double-correlated mode: turning on the current with a negative voltage on the gate is followed by a first reading of the current, a clearing of the signal charge in the internal gate with a positive pulse at the clear contact, and a second current reading before the current is turned down again and reading is switched to the next row. The difference in the first and second current reading is a measure of the signal charge in the pixel cell.

Alternative to the procedure described above, sources may be connected column-wise and source voltages measured instead of drain currents.

Fig. 21 shows the spectroscopic quality already reached with a 64 × 64 DEPFET matrix of 50 µm × 50 µm pixel size. The production of 80 mm × 80 mm devices with circular DEPFETs and of 13 mm × 100 mm matrices with linear geometry is in preparation.

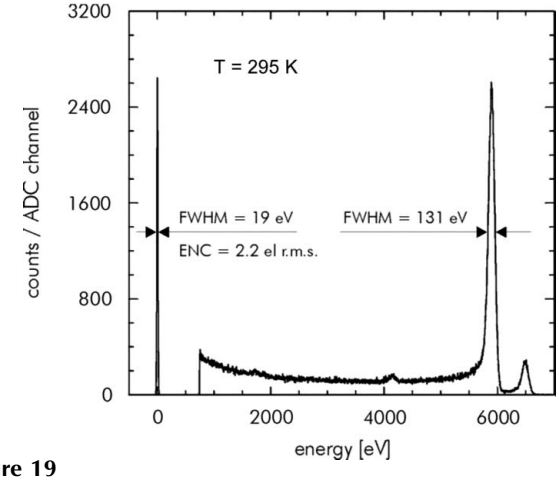

Figure 19
[55]Fe spectrum measured with a single circular (XEUS-type) DEPFET. A noise figure of 2.2 electrons r.m.s. has been obtained with room-temperature operation and 6 µs Gaussian shaping.

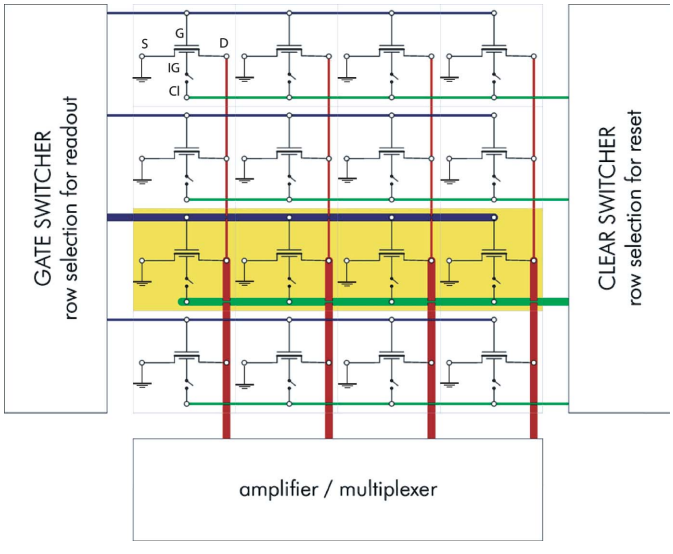

Figure 20
Circuit diagram of a DEPFET pixel detector with parallel row-wise readout of the drain current.

7. Macro pixel sensors

Pixel sensors with very large pixel sizes can be constructed by combining the DEPFET structure with the drift chamber principle. Large pixel sizes may be preferred in order to achieve an increase of readout speed and a reduction in the number of electronic readout channels and in power consumption. In any case it is advisable to match the pixel size to the properties of the rest of the system. Over-sampling may even increase the electronic noise and lead to a worsening of performance.

Fig. 22 shows the principle with a cut and a top view of a cell. The circular DEPFET structure is located in the centre of a cylindrical drift detector. Electrons created anywhere in the fully depleted bulk are driven by the suitably shaped drift field towards the internal gate below the transistor channel. For this device a new type of DEPFET has been invented that allows clearing of the signal charge with substantially lower voltage by putting the clear electrode inside the drain region located in the centre. The drain region does not consist of a highly doped p-region but is formed by an inversion layer that is controlled by a gate voltage and automatically connected to the small drain contact. By changing this gate voltage sufficiently far in the positive direction, the drain disappears and

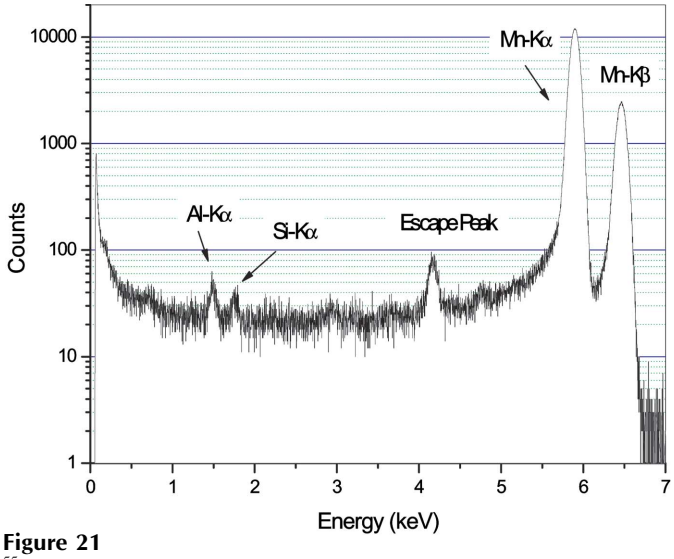

Figure 21
[55]Fe energy spectrum measured at 245 K with a 64 × 64 cell prototype DEPFET pixel matrix with 50 µm pixel size.

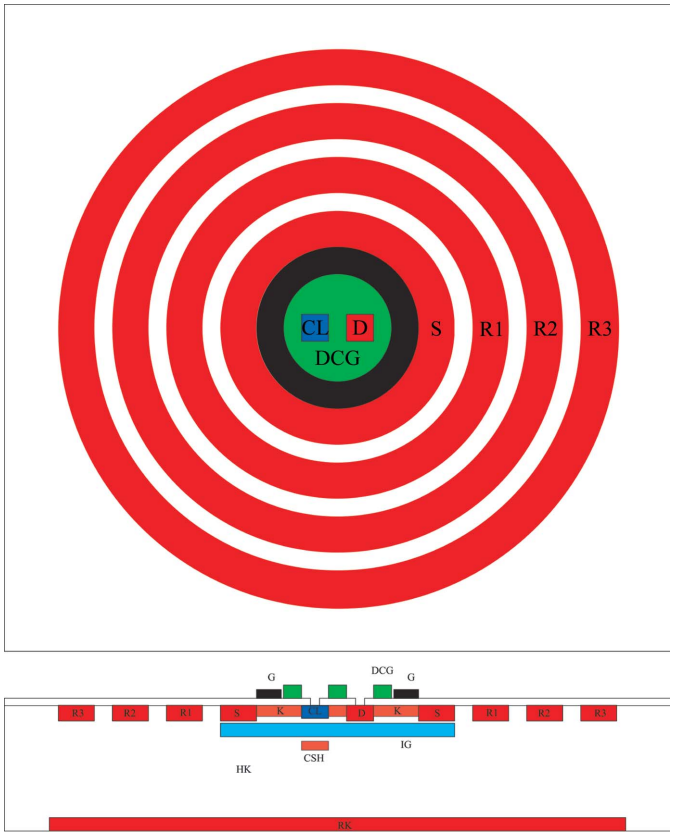

Figure 22
Principle of a macro-pixel cell: a DEPFET located at the centre of a drift detector serves as storage and readout device. A new type of DEPFET has been implemented.

assumes the role of the clear electrode, being automatically connected to the n-doped clear contact.

Single-pixel cells and 4 × 4 as well as 8 × 8 prototype pixel matrices with 1 mm × 1 mm pixel size (Fig. 23) have been tested successfully in the laboratory. Fig. 24 shows a ^{55}Fe spectrum taken at room temperature. Here one notices a somewhat worse spectroscopic resolution than with the high granular pixel devices. This is due to the leakage current which is now collected from a volume increased by a factor of 400. The leakage current can be suppressed by lowering the operating temperature.

8. Application of semiconductor (silicon) detectors in synchrotron radiation experiments

The detectors described in this article have been developed for applications in X-ray astronomy and in particle physics. Naturally there are different requirements to be met in the different fields of research. Generally one may say that, even within a field of research, requirements vary a lot for specific experiments. Properties of detectors may also be adapted to specific requirements by changing the layout but still keeping the basic function principle.

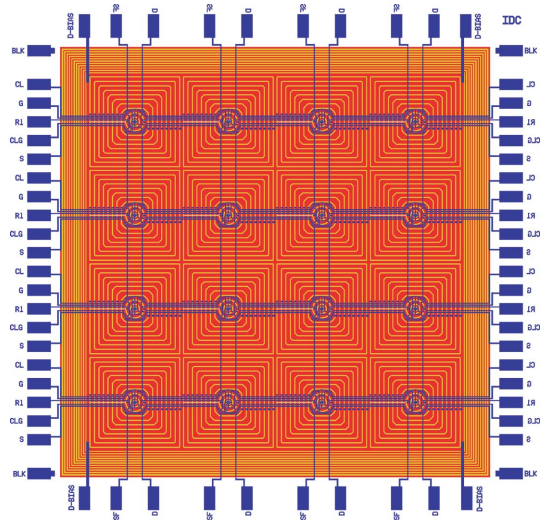

Figure 23
Layout of a 4 × 4 prototype macro-pixel matrix.

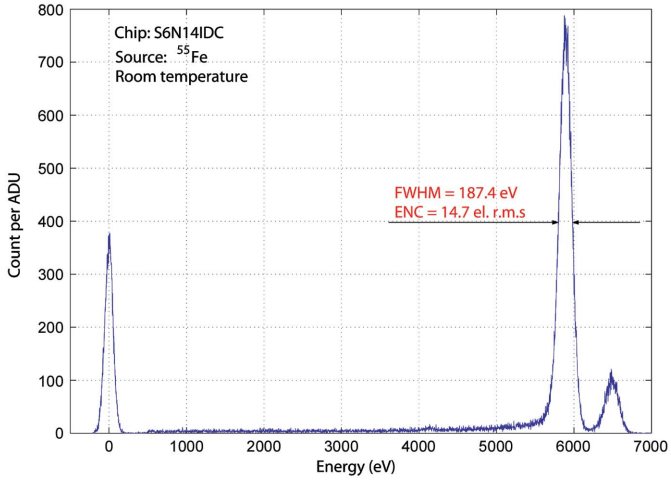

Figure 24
^{55}Fe spectrum measured at room temperature in a 1 mm × 1 mm pixel of an 8 × 8 macro-pixel matrix with 6 µs continuous shaping. The increase in the noise compared with single DEPFET cells is due to the leakage current in the large sensitive volume of 1 mm × 1 mm × 0.45 mm. That can be reduced by cooling the device.

One important parameter is the energy range. Silicon, the only detector material considered in this article, covers an energy range up to roughly 20 keV in which the absorption probability, and therefore the detection probability, remains high. Higher energies can be detected with other materials like germanium, GaAs and CdTe. Germanium has to be cooled due to the small band gap, and for compound semiconductors there are still problems with purity and defects. Furthermore, processing technologies are by far not as mature as with silicon.

A very promising method for extension of the energy range is the combination of multichannel silicon drift detectors with scintillating crystals. There the photon energy is converted to light which then spreads to several drift detector cells. The excellent charge measurement capability of the drift detectors allows an accurate determination of the position of the

interaction point and a good measurement of the photon energy.

Advantages for synchrotron applications of the current systems are:

(i) The use of an area detector with energy-resolving capabilities would allow for instance to discriminate against a fluorescence background in diffraction experiments. It would reduce the background and thus increase the signal-to-noise ratio. This is particularly advantageous in multiwavelength anomalous diffraction experiments on proteins at wavelengths above the absorption edge, where there is a natural increase in the fluorescence background. Also, in diffuse scattering experiments, where the signal is weak and spread out, the energy-resolving capability could have major advantages.

(ii) Another obvious advantage is the increase in solid collection angle in spectroscopy experiments, thereby making a much more efficient use of the available photons. This is particularly important in experiments with biological samples, which suffer from severe radiation damage, and thus have a limited lifetime. Of course one might also use the angular distribution profile of the fluorescence signal, for instance in fluo-holography experiments.

(iii) The DEPFET pixel detector principle that avoids the necessity of shifting charge towards a readout node would allow for uninterrupted data collecting, eliminating the need for X-ray shutters and the start–stop–start mode of data collecting currently used in the case of MOS-CCD-based detectors. This will not only result in faster data collecting, but almost certainly also in better data, since it eliminates mechanical operations like opening and closing of X-ray shutters, synchronized with accelerating and decelerating sample motions.

The detectors described above are usually employed for the measurement of single photons in the X-ray range. Precision measurement of photon energies requires measurement time, typically of the order of microseconds. Therefore one is limited in the data-collecting rate. If signals are spread smoothly over the detector area, this problem can be alleviated by increasing the granularity of the detectors.

If, as is frequently the case in synchrotron experiments, the X-rays are concentrated on distinct positions and, in addition, the intensity at these points differs by orders of magnitude, then increasing of granularity is not a solution. Here it may be advantageous to forget about measurement of individual photon energies and look at total collected charge only. For mono-energetic X-rays this is almost equivalent to counting the number of photons, since the low electronic noise of high-quality semiconductor detector systems can be neglected in comparison with the contribution of the statistical fluctuation of the energy-to-charge conversion process. The average number N of generated charge carriers per incident photon of energy E and its statistical fluctuation due to the energy-to-charge conversion process is described by the Fano relations

$$N = E/\varepsilon \quad \text{and} \quad \sigma_F = (FE/\varepsilon)^{1/2} = (FN)^{1/2},$$

where E is the photon energy, ε is the average energy needed to create one electron–hole pair (= 3.65 eV for silicon at room temperature) and F is the fano factor (= 0.125 for silicon). The number of electrons nN created by n photons with the same energy E then gives a statistical fluctuation of

$$\sigma_F(nN) = (nFE/\varepsilon)^{1/2} = (nFN)^{1/2}.$$

An additional contribution to this fluctuation of signal charge comes from the electronic noise with its equivalent noise charge σ_q.

Converting now to the number of photons, one divides by the number of electrons per interacting photon N and arrives at the statistical fluctuation for the measurement of the number of interacting photons,

$$\sigma(n) = \left[\sigma_F^2(n) + \left(\sigma_q/N\right)^2\right]^{1/2} = \left[(F/N)n + \left(\sigma_q/N\right)^2\right]^{1/2}.$$

Taking as numerical examples an electronic noise of $\sigma_q = 10$ electrons and photon energies of 300 eV and 10 keV corresponding to generated electrons per photon of 83 and 2780, respectively, one obtains an uncertainty in the number of photons of

$$\sigma(n) = [0.0392n + 0.0122]^{1/2}$$

for E = 300 eV and

$$\sigma(n) = \left[\left(6.75 \times 10^{-3}\right)^2 n + \left(3.6 \times 10^{-3}\right)^2\right]^{1/2}$$

for E = 10 keV. For the high-energy example one needs to measure 22000 events to make an error of one photon; for the low-energy example 650 events are required.

Comparing this method of accumulated charge measurement to the often proposed procedure of simply counting the number of signals above a set threshold within each pixel, one has also to consider the consequences of the splitting of signal charge between neighboring pixels that is impossible to prevent. While for the charge sum measurement charge splitting is not a problem, it may lead to double counting and/or inefficiencies in the digital counting method, depending on the actual choice of the energy threshold and by the statistical fluctuation of the individual photon conversions. It should be noted furthermore that photon counting does not work for very high rates as photons have to be separated from each other sufficiently in time to allow the individual application of a threshold comparison to each photon signal. This task is avoided by the measurement of total accumulated pixel charge and photon numbers can be measured even for pulses in the femtosecond range as will be the case in the free-electron laser facilities.

Furthermore, as shown above, photon number measurement will in almost all high-rate conditions be more precise than counting signals above threshold and always way below the Poissonian statistics of the processes to be investigated.

I am indebted to many colleagues and in particular those from the MPI Semiconductor Laboratory for help and for providing partially unpublished material for this article.

References

Fiorini, C., Longoni, A., Boschini, L., Perotti, F., Labanti, C., Rossi, E., Lechner, P. & Strüder, L. (1999). *IEEE Trans. Nucl. Sci.* NS-**46**, 858–864.

Fiorini, C., Longoni, A., Perotti, F., Labanti, C., Rossi, E., Lechner, P., Soltau, H. & Strüder, L. (2002). *IEEE Trans. Nucl. Sci.* **49**, 995–1000.

Gatti, E. & Rehak, P. (1984). *Nucl. Instrum. Methods*, **225**, 608–614.

Gauthier, Ch., Goulon J., Moguiline, E., Rogalev, A., Lechner, P., Strüder, L., Fiorini, C., Longoni, A., Sampietro, M., Walenta, A., Besch, H., Schenk, H., Pfitzner, R., Tafelmeier, U., Misiakos, K., Kavadias, S. & Loukas, D. (1996). *Nucl. Instrum. Methods*, A**382**, 524–532.

Hartmann, R., Hauff, D., Krisch, S., Lechner, P., Lutz, G., Richter, R. H., Seitz, H., Strüder, L., Bertuccio, G., Fasoli, L., Fiorini, C., Gatti, E., Longoni, A., Pinotti, E. & Sampietro, M. (1994). *IEDM Tech. Dig.* pp. 535–539.

Hartmann, R., Strüder, L., Kemmer, J., Lechner, P., Fries, O., Lorenz, E. & Mirzoyan, R. (1997). *Nucl. Instrum. Methods*, A**387**, 250–254.

Kemmer, J. & Lutz, G. (1987*a*). *Nucl. Instrum. Methods*, A**253**, 365–377.

Kemmer, J. & Lutz, G. (1987*b*). *Nucl. Instrum. Methods*, A**253**, 378–381.

Kemmer, J. & Lutz, G. (1988). *Nucl. Instrum. Methods*, A**273**, 588–598.

Kemmer, J., Lutz, G., Belau, E., Prechtel, U. & Welser, W. (1987). *Nucl. Instrum. Methods*, A**253**, 378–381.

Kemmer, J., Lutz, G., Prechtel, U., Schuster, K., Sterzik, M., Strüder, L. & Ziemann, T. (1990). *Nucl. Instrum. Methods*, A**288**, 92–98.

Lechner, P., Pahlke, A. & Soltau, H. (2003). Presented at the *European Conference on Energy-Dispersive X-ray Spectrometry (EDXRS 2002)*, Berlin, Germany, 17–21 June 2002. To be published.

Meidinger, N., Bräuninger, H., Briel, U., Hartmann, R., Hartner, G., Holl, P., Kemmer, J., Kendziorra, E., Krause, N., Lutz, G., Pfeffermann, E., Popp, M., Reppin, C., Richter, R., Soltau, H., Stötter, D., Strüder, L., Trümper, J. & von Zanthier, C. (1999). *Proc. SPIE*, **3765**, 192–203.

Meidinger, N. *et al.* (2006). *Nucl. Instrum. Methods Phys. Res. A*. To be published.

Pinotti, E., Bräuninger, H., Findeis, N., Gorke, H., Hauff, D., Holl, P., Kemmer, J., Lechner, P., Lutz, G., Kink, W., Meidinger, N., Metzner, G., Predehl, P., Reppin, C., Strüder, L., Trümper, J., Zanthier, C. v., Kendziorra, E., Staubert, R., Radeka, V., Rehak, P., Bertuccio, G., Gatti, E., Longoni, A., Pullia, A. & Sampietro, M. (1993). *Nucl. Instrum. Methods*, A**326**, 85–92.

Radeka, V., Rehak, P., Rescia, S., Gatti, E., Longoni, A., Sampietro, M., Bertuccio, P., Holl, P., Strüder, L. & Kemmer, J. (1989). *IEEE Elec. Dev. Lett.* **10**, 91–95.

Strüder, L., Englhauser, J., Hartmann, R., Holl, P., Meidinger, N., Soltau, H., Briel, U., Dennerl, K., Freyberg, M., Haberl, F., Hartner, G., Pfeffermann, E., Stadlbauer, T. & Kendziorra, E. (2003). *Nucl. Instrum. Methods*, A**512**, 386–400.

Strüder, L., Holl, P., Lutz, G. & Kemmer, J. (1987). *Nucl. Instrum. Methods*, A**257**, 594–602.

XEUS (1999). *X-ray Evolving Universe Spectroscopy – The XEUS Scientific Case*, ESA SP-1238. European Space Agency, Paris, France.